A 3C/3D SEISMIC ANALYSIS OF THE APPALACHIAN BASIN HAMILTON GROUP, NORTHEASTERN PENNSYLVANIA

MICHAEL V. DEANGELO and BOB A. HARDAGE

Bureau of Economic Geology, John A. and Katherine G. Jackson School of Geosciences, The University of Texas at Austin, Austin, TX 78713-8924, U.S.A. mike.deangelo@beg.utexas.edu

(Received July 10, 2012; revised version accepted April 18, 2013)

ABSTRACT

DeAngelo, M.V. and Hardage, B.A., 2013. A 3C/3D seismic analysis of the Appalachian Basin Hamilton Group, Northeastern Pennsylvania. *Journal of Seismic Exploration*, 22: 271-293.

A 3D multicomponent seismic study was initiated in Northeastern Pennsylvania to determine if these emerging technologies could improve the geological understanding of the Appalachian Basin Hamilton Group with regards to hydrocarbon exploration and waste-storage management. By comparing conventional P-P wave data with P-SV wave data, it was demonstrated that these concepts could help reduce exploration risk and minimize environmental impact by improving reservoir characterization, identifying possible zones of increased fracture density, and help locate potential subsurface waste-water intervals to safely store any fluid generated from drilling activities in environmentally sensitive areas.

KEY WORDS: 3C/3D seismic, interpretation, fractures, anisotropy, Marcellus shale, Tully/Tichenor sandstones.

INTRODUCTION

The 3D multicomponent (3C/3D) seismic data used in this study were acquired as multi-client lease data. The study area was in Bradford County, Northeastern Pennsylvania, where recent interest in the Marcellus Shale has led to extensive drilling for hydrocarbon resources (Engelder et al., 2009). The Hamilton Group is bounded by the Tully (youngest) and Onondaga (oldest) limestones, which were deposited in a deep-water oxygen-free environment during the Middle Devonian (Roen, 1984; Soeder, 1988). The Marcellus Shale

0963-0651/13/$5.00

within the study area is a thin (approximately 90 m), organically rich formation within the Hamilton Group and is a significant shale-gas reservoir (Hill, 2002). We used 3C/3D seismic data to improve reservoir characterization of the Marcellus Shale and help identify potential reservoirs throughout the interval that could be used for subsurface storage of waste-water generated from drilling activities.

The seismic survey (Fig. 1) was an orthogonal brick pattern in which 13 receiver lines spaced 880 ft (268 m) apart were deployed northwest-to-southeast to form a 2 mi - 2 mi (3.2 km - 3.2 km) square of 3C microelectromechanical systems (MEMS) accelerometer stations, with 97 receiver stations spaced at intervals of 110 ft (33.5 m) along each receiver line. The total number of planned receiver stations was 1261. This receiver grid was to be positioned in the center of a 5 mi - 5 mi (8 km - 8 km) square array of source stations arranged in a southwest-to-northeast brick pattern in which 41 source lines were spaced 660 ft (201 m) apart. Each source line consisted of a sequence of four source stations spaced at intervals of 220 ft (67 m) with a gap of 880 ft (268 m) between successive 4-station groups. This source-station pattern created 60 source stations per line, with a total of 2460 source points across the survey area. Each source involved a 2.2 lbs (1 kg) explosive positioned at a depth of 20 ft (6 m).

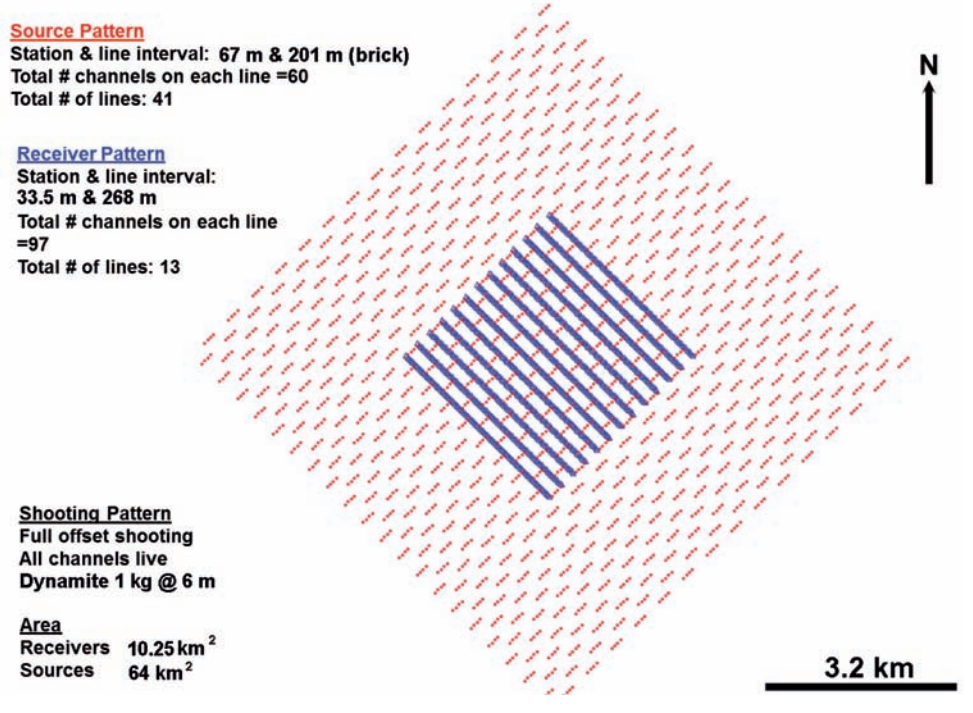

Fig. 1. 3C/3D seismic acquisition survey preliminary design.

The data were processed to produce three time-migrated data volumes - a conventional P-wave (P-P) volume, a fast-S converted wave (P-SV_1) volume, and a slow-S converted (P-SV_2) volume. Each data volume consisted of 30,448 data traces. Data traces were 4 seconds long. Image bin dimensions were 110-ft - 110-ft (33.5-m - 33.5-m). The seismic images spanned an area of approximately 6 mi^2 (23.8 km^2).

Important geologic calibration data were recorded in a well positioned at the center of the seismic image space spanned by the 3D data volumes. Vertical seismic profile (VSP) data acquired in this calibration well were invaluable for depth registering P and S seismic data. Additional calibration data acquired in this central-image well were a full suite of modern logs that provided rock and fluid properties needed for modeling P and S reflectivities. A log of particular value was the dipole-sonic log, which measured P, fast-S, and slow-S velocities, indicated fast-S and slow-S polarization azimuths, and estimated P-SV wave anisotropy. These dipole-sonic log data were used to generate P-wave and P-SV wave synthetic seismograms that aided depth registration of P-P and P-SV data and identified key geologic targets in seismic images. As a result of having high-quality geologic calibration data, we achieved robust time-to-depth correlations of geology with P-P, P-SV_1, and P-SV_2 images.

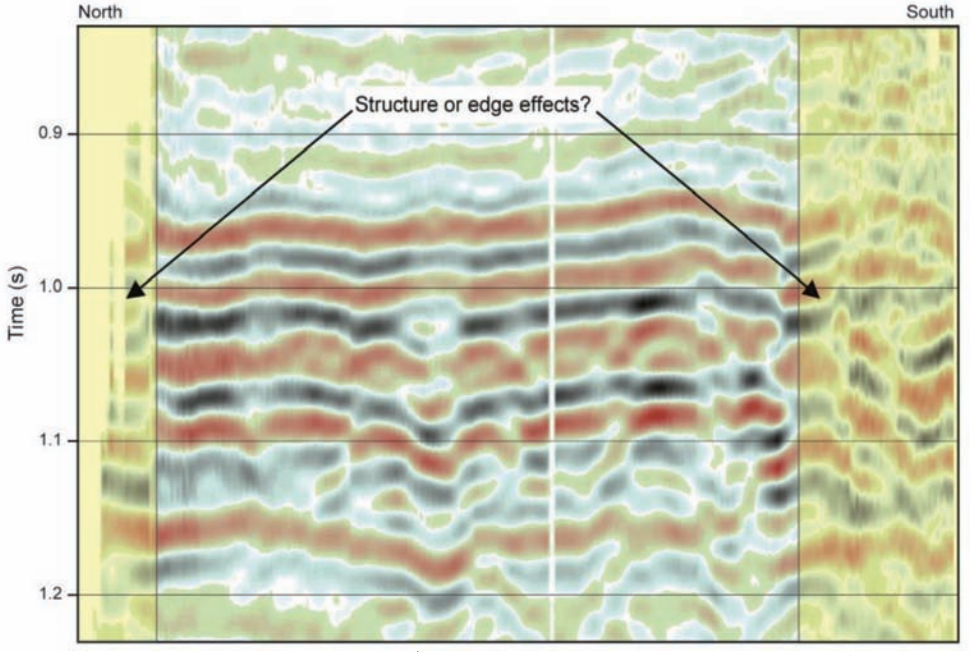

Fig. 2. Profile showing processing artifacts (shaded areas) along the edges of P-P image space.

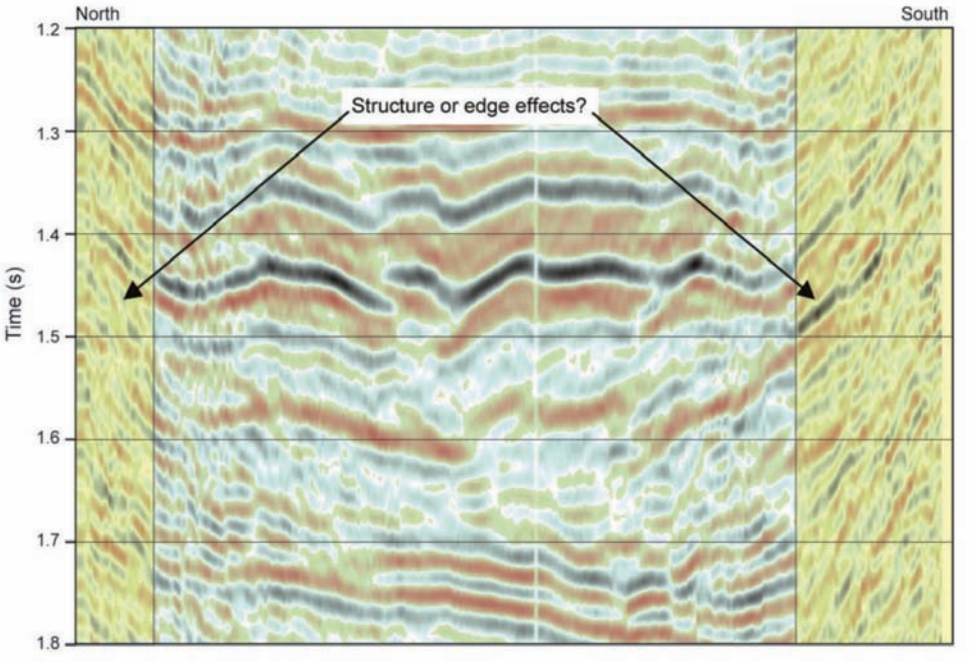

Fig. 3. Same profile as (a) showing processing artifacts (shaded areas) along the edges of P-SV_1 (fast-S) image space. Note the increase in reflection dip inside the shaded areas.

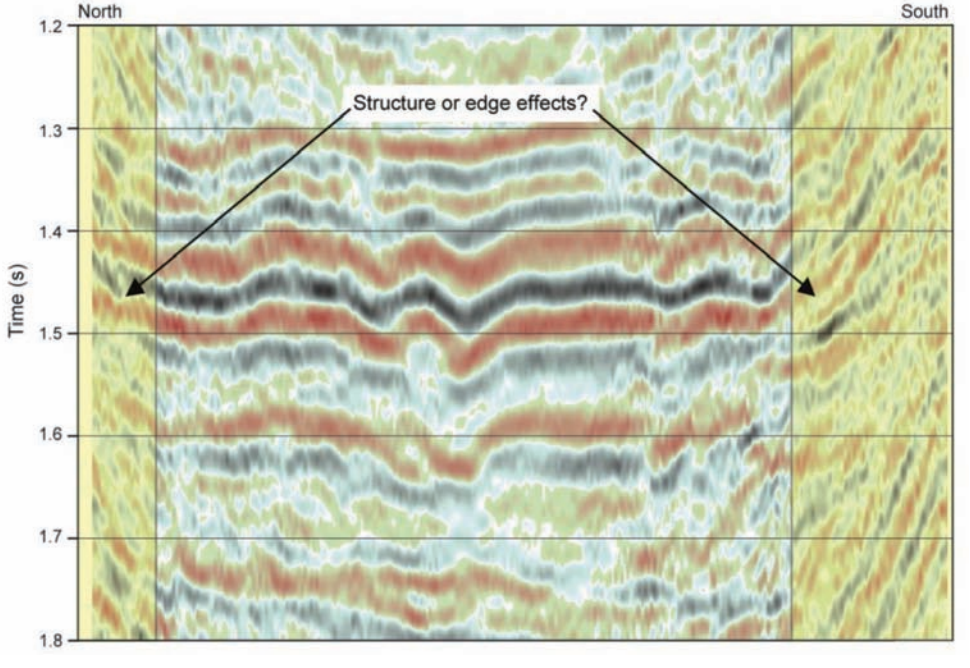

Fig. 4. Same profile as (a) showing processing artifacts (shaded areas) along the edges of P-SV_2 (slow-S) image space. Note the increase in reflection dip inside the shaded areas.

Seismic data quality

Analysis of P-P, P-SV_1, and P-SV_2 data volumes showed P-SV wave data volumes were more distorted by irregularities along the edges of image space than was the P-wave volume. These P-SV processing artifacts produced greater apparent structural dips, as well as more reflection smearing, than were present in the P-P volume (Figs. 2, 3, 4). All three data volumes had small blank-out areas inside the image space where landowners would not grant permission for their subsurface to be leased. To protect these no-permit areas, data across these no-lease properties were deleted from each data volume. To ensure these data gaps created no processing artifacts, data were deleted after, not before, wavefield migration.

Frequency spectra analysis

The profiles shown on Figs. 2 through 4 compare the vertical resolution for P-P, P-SV_1 and P-SV_2, respectively. Spectral analyses of all three time-domain volumes confirmed the frequency content of each 3D image was reasonably broad band. The P-P data volume had a rather flat frequency spectrum between 10 and 40 Hz, with energy content then steadily reducing to -40 dB at 80 Hz (Fig. 5a). Both P-SV modes (P-SV_1 and P-SV_2) had spectra that were approximately flat from 8 to 35 Hertz, with reduced, but significant, energy content extending to almost 55 Hz (Figs. 5b and 5c). The spectra shown on Fig. 5 were calculated for trace lengths that extended from the Earth surface to slightly below what was interpreted to be seismic basement in each image space.

METHODS

Time to depth calibration

Before seismic interpretation was initiated, it was essential to determine which reflection events correlate with key geologic horizons. When interpreting 3C/3D seismic data, time-to-depth calibrations must be established for P-P data and for each P-SV mode involved in an interpretation. Data acquired in our central-image calibration well allowed two approaches to be implemented to establish time-to-depth correlations for the seismic data. The first approach was to utilize synthetic seismograms; the second approach was to use VSP time-based and depth-based images. We utilized the simpler, and more common, option generating synthetic seismograms constructed from dipole sonic logs combined with VSP check-shot controls to establish accurate transformations from log depth to seismic-image time.

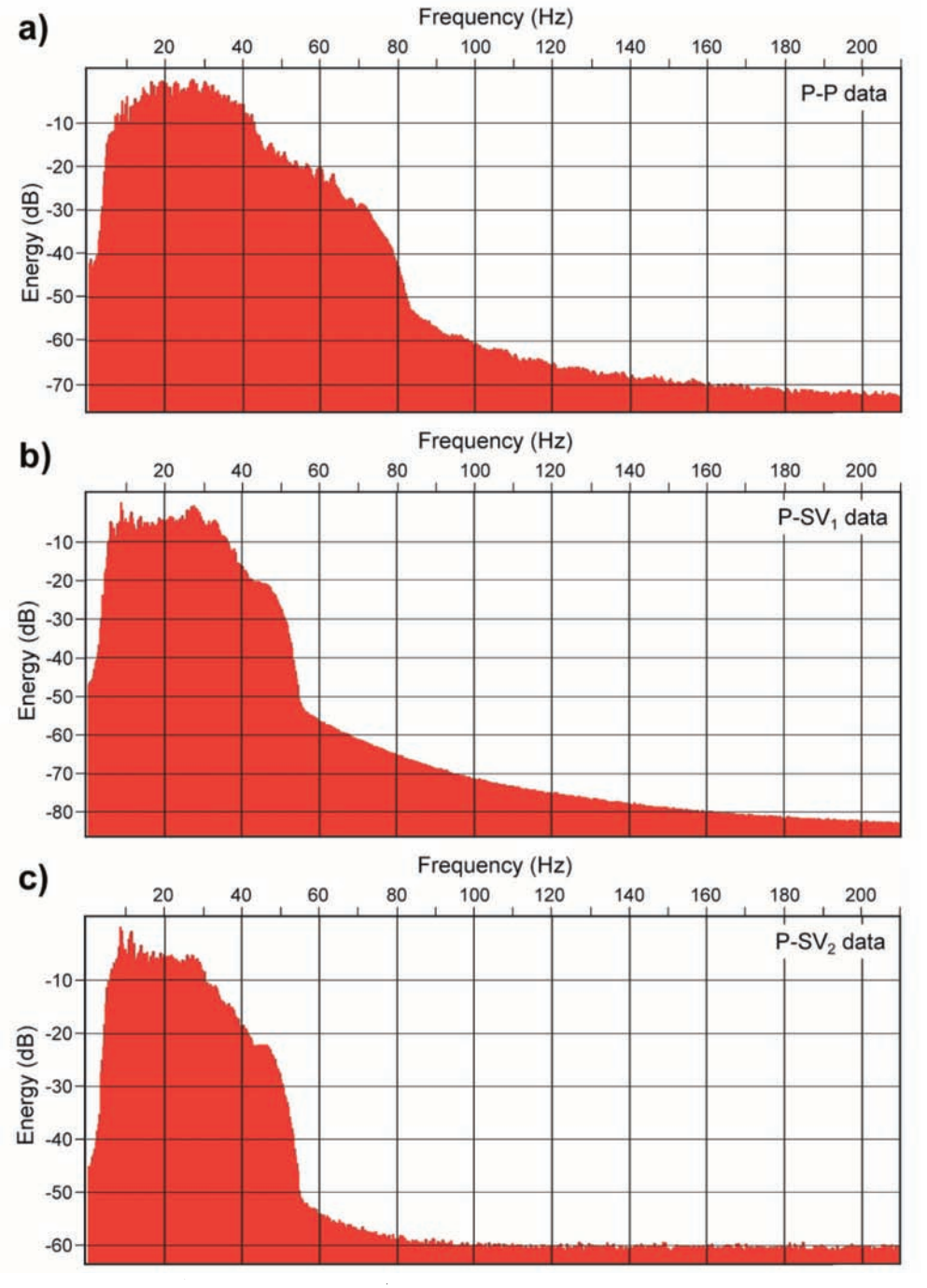

Fig. 5. Frequency spectrum of: (a) P-P, (b) P-SV_1 (fast-S), and (c) P-SV_2 (slow-S) data.

Velocity logs recorded in the central-image calibration well provided depth profiles of both P-wave velocity (VP) and P-SV wave velocity (VS). P-P and P-SV_1 synthetic seismograms were calculated by combining these velocity logs with the density log from the calibration well. These synthetic seismograms were our principal approach to defining depth-equivalent P and S reflection events as 3D P-P and P-SV data volumes were interpreted. The VSP-based calibration, utilizing check-shot control points, of log depth to seismic time defined depth-equivalent P and S horizons with high confidence.

Additional confirmations of the accuracies of correlations between depth-based geology and time-based P-P and P-SV images are shown on Fig. 6 where the gamma-ray log recorded in the calibration well is displayed atop time-migrated P-P data (Fig. 6a), P-SV_1 data (Fig. 6b), and P-SV_2 data (Fig. 6c). In each display, the depth-based gamma-ray curve is adjusted to the respective seismic image time using VSP time-depth information measured from VSP data acquired in the calibration well. Each significant change in gamma-ray magnitude correlates with a specific reflection event that allows depth-equivalent horizons in each volume to be defined.

The calibration well was drilled only to the Onondaga, immediately below the Marcellus, because the well was to be completed as a horizontal well in the Marcellus Shale. Thus log-based and VSP-based calibration of seismic data terminated at the top of the Onondaga Sandstone. The position of the deeper Oriskany unit shown on Fig. 6 is speculative. The depth of the Oriskany at the

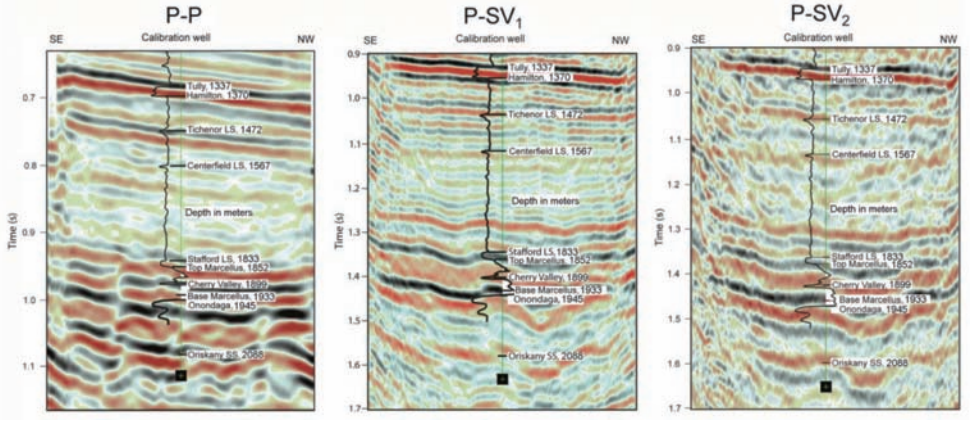

Fig. 6. (a) Time-migrated P-P data with gamma-ray log from the calibration well adjusted to VSP-defined P-P image time, (b) Time-migrated P-SV_1 data with gamma-ray log from the calibration well adjusted to VSP-defined P-SV_1 image time and, (c) Time-migrated P-SV_2 data with gamma-ray log from the calibration well adjusted to VSP-defined P-SV_2 image time.

calibration well was estimated by gridding and contouring known interpreted tops from regional wells that penetrated the Oriskany. The resulting contour map extrapolated these control points to the area where the calibration well was positioned. As a result, the seismic reflection feature labeled "Oriskany 2088" on each image is only an estimate of the measured depth (meters) of the Oriskany at the calibration well.

Interpreting depth-equivalent P- and S-horizons

The greatest problem confronting interpreters of 3C/3D seismic data is to determine which P-SV reflection is equivalent to a targeted P-P reflection event. The importance of accurate correlation between 3C/3D data cannot be over-emphasized. Until equivalent P-P and P-SV horizons are established, seismic attributes cannot be compared across targeted stratigraphic intervals to determine attribute combinations that optimize the detection of specific rock and fluid properties.

A common approach to determining equivalent events in 3C/3D data volumes is to work in section views, using procedures similar to those followed when interpreting 2D seismic profiles (Tatham and McCormick, 1991; DeAngelo et al., 2003). This vertical-section approach to interpreting 3C/3D seismic data is satisfactory if adequate precautions are taken to ensure miscorrelations of key stratal surfaces do not occur. We think our time-depth registration of P-P and P-SV data is accurate because our definitions of depth-equivalent horizons were established using travel times observed in VSP data acquired in the central-image calibration well. P-P and P-SV traveltimes to key depth-based stratigraphic horizons penetrated by this VSP calibration well were marked at the well X-Y coordinates in each time-based data volume to define the P-P and P-SV reflection event associated with that horizon. Each horizon was then extended from this well-control point across all of P-P and P-SV image space.

Away from the VSP calibration well, inline and cross-line sections of P-P and P-SV data were compared to define characteristic features that should be expected on both data sets and which would increase confidence that depth-equivalent horizons were being followed as interpretation proceeded farther from the VSP calibration well. Geometric features such as stratigraphic terminations and lap-outs, if observed in both P and S image space, were important for deciding how to constrain the interpretation to depth-equivalent P and S horizons. However, P-SV seismic sequences often differ from P-P seismic sequences so this interpretation guideline must be used with discretion.

An attempt was made to use fault surfaces for depth correlation. If faults cut across reflections at significant angles away from vertical, it is often possible

to match depth-equivalent breaks in reflections. In such cases, interpreted horizons can be verified as being depth equivalent by comparing fault maps of these interpreted horizons. In contrast, if faults are near-vertical, it is difficult to decide how much vertical shift should be applied to a P-SV wave profile to make a P-SV horizon depth-equivalent to a targeted P horizon. For near-vertical faults, fault maps of P and P-SV horizons show minor changes in X-Y coordinate location over large vertical intervals of P and P-SV data windows. This focus on fault interpretation is a valuable approach to depth registration of images in both domains, but it was not productive for our study area because no significant faults were present inside our seismic image space.

Stratal slicing

A fundamental premise of seismic stratigraphy is that a seismic reflection event follows a *chronographic surface*, which is a depositional surface where geologic time does not change. Stated another way, a seismic reflection event defines a bedding surface, or *stratal surface*, which is a surface where geologic time is constant. All seismic stratigraphy studies are based on the principle that geologic time is constant along a horizon that follows a fixed seismic reflection phase. A corollary to this principle is that a seismic horizon that is conformable to a seismic reflection is also a surface along which geologic time is constant.

If the top and base of an interval is bounded by reflection events that are conformable to each other, it is rather simple to interpolate an arbitrary number of conformable horizons that span the interval between these two reflections. Seismic attributes calculated on each successive internal conformable surface describe stratigraphy within the interval at fixed increments of geologic time. A different strategy, developed by Zeng et al. (1998, 2001), must be implemented if reflection events at the top and base of an interval are not conformable. In this approach, an interval having a time-varying thickness is divided into an arbitrary number of uniformly spaced sub-intervals as shown on Fig. 7.

At any two coordinates along this profile, the vertical spacing between adjacent interpolated surfaces differs in seismic time but is constant in geologic time. The result is a series of surfaces that define depositional features within the interval at fixed increments of geologic time. The creation of the interpolated surfaces between Reflections A and B on Fig. 7 is called *stratal slicing*. In this example, the interval between Reflection A and Reflection B is divided into 11 sub-intervals. If the time interval at some point on the profile is 11 ms, each sub-interval is 1 ms thick at that image coordinate. If the interval from A to B is 110 ms thick at a second point on the profile, each sub-interval is 10 ms thick at this second image coordinate. Even though the magnitude of seismic image time spanned by each sub-interval differs at these two points, the

geologic time across each sub-interval is MY/11 at both points, where MY is the geologic time difference between Reflection A and Reflection B. Because of the interpolation technique used to create these sub-intervals, the creation of stratal slices is also called *proportional slicing*.

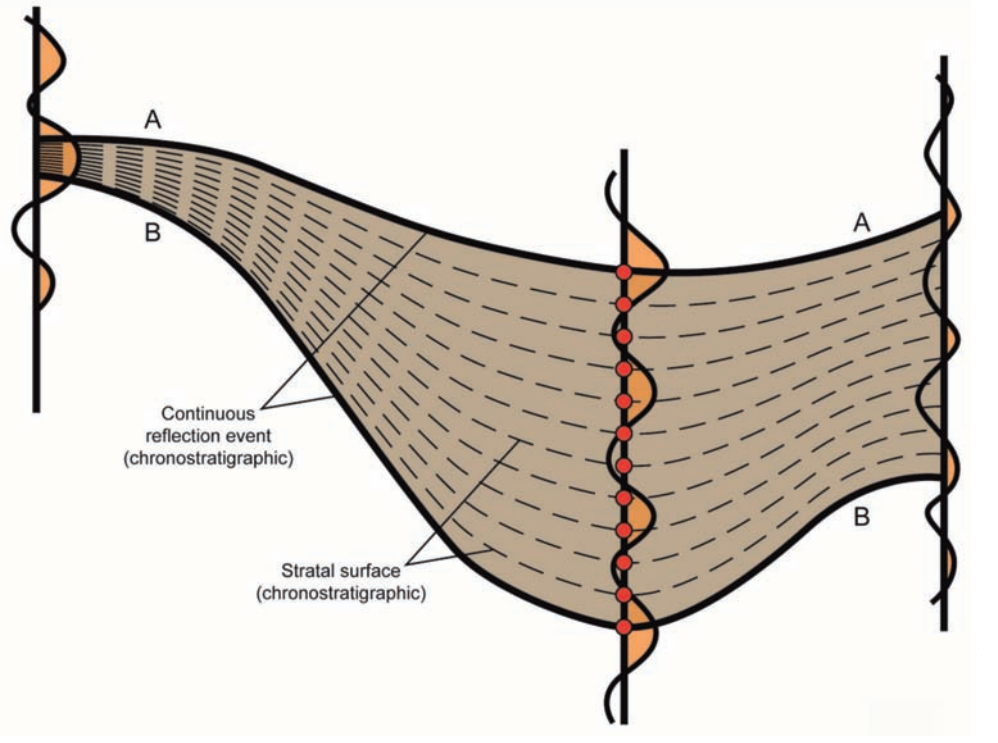

Fig. 7. Stratal slices along a seismic profile where there are significant variations in the interval thickness between two chronostratigraphic reflections (A and B).

DISCUSSION

Tully to Tichenor interval

Previous studies indicate transgressive Devonian sandstones are often found in the stratigraphic interval immediately below the Tully Limestone (Bruner and Smosna, 1994; Diecchio, 1985; Milici and Swezey, 2006). Because porous, brine-filled sandstones are good candidates for water-storage reservoirs, we did a detailed interpretation of the interval between the interpreted tops of the Tully Limestone and Tichenor Limestone to determine how P and S seismic data react to these particular sandstone targets.

Time windows chosen for spectral analysis of the Tully-to-Tichenor interval for P-P, P-SV_1, and P-SV_2 data are shown on Fig. 8, respectively. The Tully unit is characterized by a strong reflection peak (black) immediately followed by a high-amplitude wavelet trough (red) in all three data volumes and is easily mapped across the image area. In contrast, the Tichenor Limestone appears as a modest-amplitude reflection in the P-P data volume, and has an even lower amplitude response in both the P-SV_1 data and the P-SV_2 volumes. Despite these weaker expressions of the Tichenor unit, depth-equivalent Tichenor horizons were interpreted across the image space in all three data volumes. Visual inspection of these side-by-side data windows leads to an important research finding - *P-SV data provide better resolution of stratigraphy across our study area than do P-P data*. An important implication is that this same advantage of P-SV wave data may occur across many shale-gas prospects.

P-P data show a marked decrease in the number of reflection cycles across the transgressive sandstone interval relative to the number of reflection cycles appearing in P-SV_1 and P-SV_2 images, allowing more interpretation detail within the interval of interest. The stratal time slicing technique was applied to the Tully-to-Tichenor interval to expand knowledge of the internal architecture

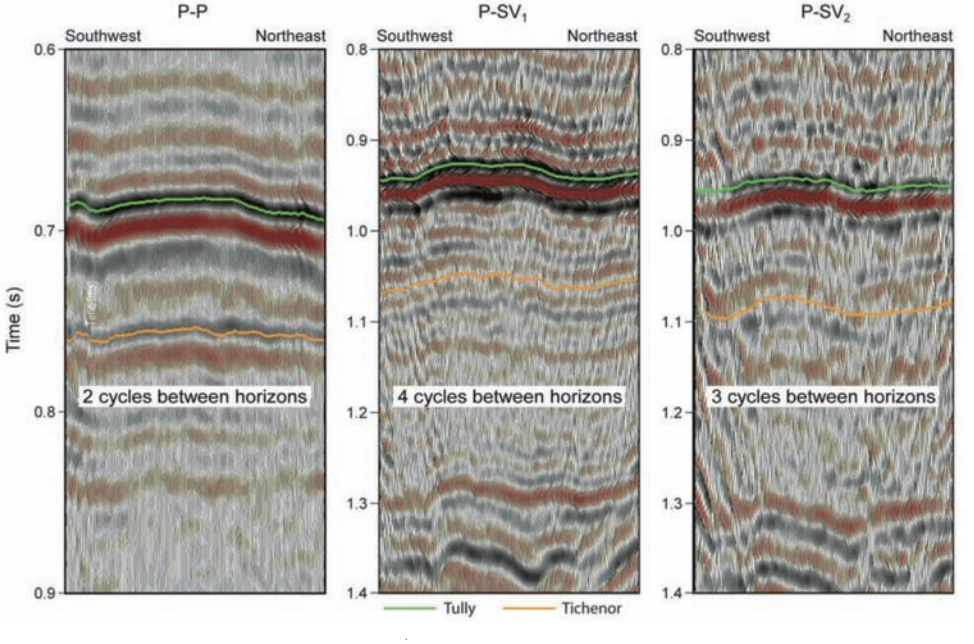

Fig. 8. Profiles comparing Tully (green horizon) to Tichenor (orange horizon) intervals in (a) P-P, (b) P-SV_1, and (c) P-SV_2 image space.

of rock units that might be used for injecting hydrofrac flow-back water. All three data volumes (P-P, P-SV_1, and P-SV_2) were analyzed. Interpreted Tully and Tichenor horizons defined on Fig. 8 were used as bounding seismic reflections to guide the stratal slicing. Example stratal slices from the volumes are exhibited on Fig. 9. Stratal slicing shows a clear bifurcation of the feature at the northeast edge of the image space. This stratal-slice interpretation adds credence to the assumption that the channel-like feature contributes to reservoir compartmentalization. The interpretation also verifies the following important concept of elastic wavefield seismic stratigraphy - one or more key depositional features not seen by one wave mode may be seen by another wave mode. In this instance, P-SV wave data see a feature that P-wave data do not see. In other instances, P-wave data will see features that P-SV wave data do not see.

An important research finding was that P-SV_1 data imaged a southwest to northeast trending feature within the Tully-to-Tichenor interval that appears similar to an eroded channel. However, the feature has no meandering character, and its linear geometry suggests there may be a genetic relationship to structure. This feature was not revealed by either P-P data or P-SV_2 data. These amplitude-attribute comparisons are an example of the increased geological information provided by elastic wavefield seismic stratigraphy (joint interpretation of P-P and P-SV data) compared to the amount of information provided by traditional seismic stratigraphy (which uses only single-component P-wave data). The erosion-like feature has a significant size, being approximately 0.25 mi (0.4 km) wide and extending across the full 3 mi (4.8 km) dimension of the image space.

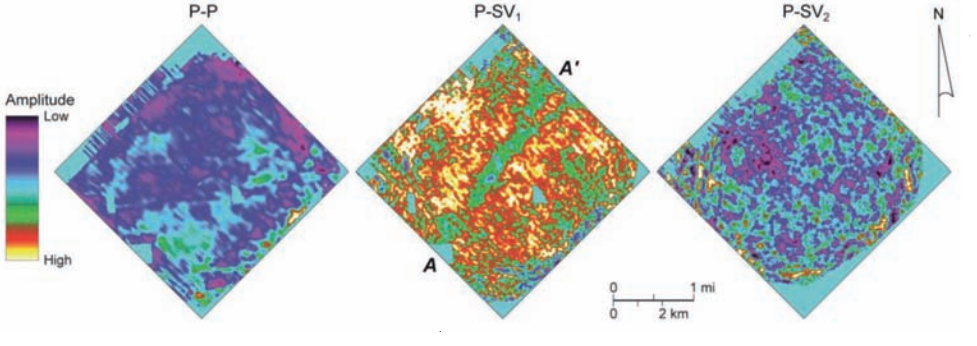

Fig. 9. Stratal slice results showing depth-equivalent surfaces within the Tully-to-Tichenor interval for the P-P, P-SV_1, and P-SV_2 stratal slices. The channel-like image labeled A-A' is a key reservoir compartmentalization feature not revealed in the other data volumes. The attributes displayed on each surface are reflection amplitude values scaled as shown by the colour bar.

The detection of this depositional feature has significant implications in evaluating water-storage reservoirs. There is not sufficient subsurface information to define the type of lithological fill within this particular geobody. Thus the feature can be a lateral barrier to fluid flow, or it could enhance fluid flow, depending on the nature of its internal lithology, porosity, and permeability. In either case, it is essential that anyone who considers Devonian sandstones within this stratigraphic interval as possible water-storage reservoirs be aware of this reservoir heterogeneity. The key point of this interpretation is that multicomponent seismic data provide a picture of reservoir compartmentalization that is not available if shale-gas operators utilize only single-component P-wave seismic data.

A second example demonstrates an instance where P-P data are more useful than P-SV_1 data for understanding the stratigraphy of the Tully-to-Tichenor interval. In this case, the number of reflection troughs within

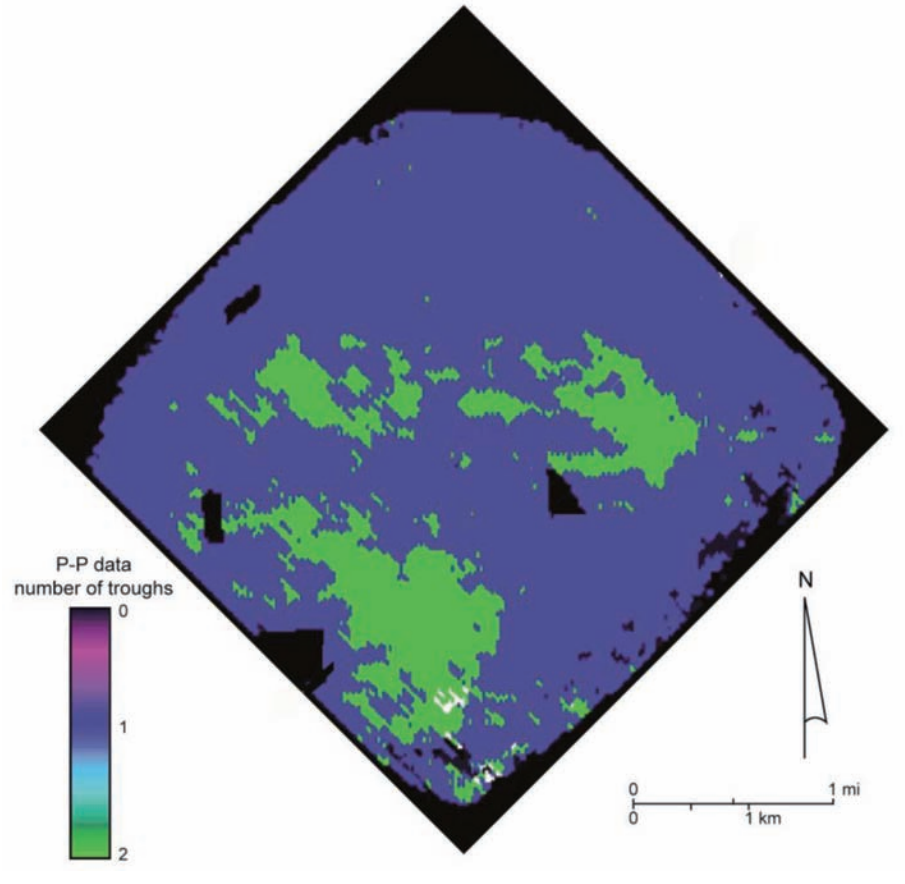

Fig. 10. Number of P-P reflection troughs across the Tully-to-Tichenor interval. In some areas, the number of troughs increases from 1 to 2.

the Tully-to-Tichenor interval was counted in P-P and P-SV_1 data sets. AlthoughP-P data had fewer reflection troughs across the interval than did P-SV_1 data, the number of P-P troughs (Fig. 10) changed in some portions of the image space, which indicates alterations in bedding thickness or bedding geometry.

Although it has been emphasized that the spatial resolution of P-P data across our study area is less than the spatial resolution of P-SV_1 data, image coordinates where changes in the number of P-P reflection troughs occur must be considered as locations where there is a change in the internal compartmentalization of the Tully-to-Tichenor interval even if P-SV_1 data show little variation at the same coordinates. Thus maps of numerical counts of reflection troughs (or peaks) across a stratigraphic interval are valuable in elastic wavefield seismic stratigraphy applications.

Marcellus shale interval

The Marcellus Shale is divided into two distinct units - the Upper Marcellus and the Lower Marcellus. The boundary between these two units is the Cherry Valley Limestone. To characterize the Marcellus interval, it was essential to accurately interpret depth-equivalent P-P and P-SV horizons that correlate with the Top of Marcellus, Cherry Valley Limestone, and Base of Marcellus. Examples of these depth-equivalent surfaces are illustrated on Fig. 11.

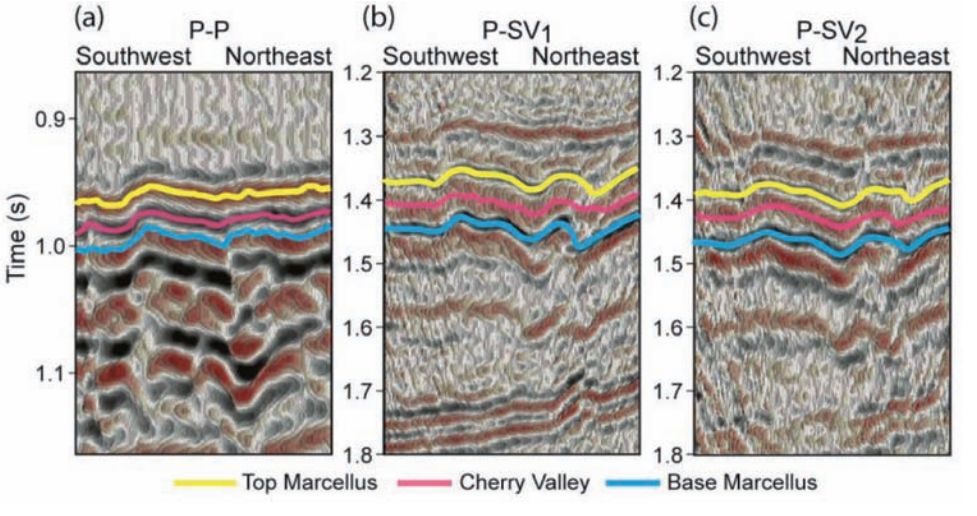

Fig. 11. Profiles showing P-P, P-SV_1, and P-SV_2 images of the Marcellus interval.

Visual inspection of the profiles displayed on Fig. 11 implies both P-SV modes have a better vertical resolution across the Marcellus interval than do P-P data. The improvement in spatial resolution provided by P-SV wave modes is another important research finding that encourages the use of multicomponent seismic technology in shale-gas studies rather than relying on only single-component P-P seismic data.

The profiles exhibited on Fig. 11 show the top and base of the Marcellus interval are associated with bold reflection events in all three data volumes. However, mapping the Cherry Valley horizon posed problems. The Cherry Valley Limestone was not imaged as an individual reflection trough or peak in any seismic data volume, making any attempt to create a Cherry Valley horizon arbitrary. Automatic picking algorithms failed to track any consistent seismic feature related to the Cherry Valley Limestone, making it necessary to find a seismic attribute that might help discriminate the Cherry Valley unit from its surrounding Marcellus Shale units. After a series of trials, it was determined instantaneous phase was the best attribute to use to define the Upper Marcellus-Cherry Valley interface.

The improved resolution of Marcellus geology provided by P-SV data compared to P-P data is more striking when wavelength spectra are considered. P-P wavelengths (λ_P) are defined as $\lambda_P = V_P/f$, where f = frequency, and P-SV wavelengths (λ_S) are defined as $\lambda_S = V_S/f$. Thus,

$$\lambda_S = \lambda_P(V_S/V_P) \quad . \tag{1}$$

Because the V_P/V_S velocity ratio within the Marcellus is approximately 1.6, this wavelength relationship simplifies to:

$$\lambda_S = 0.62\lambda_P \quad . \tag{2}$$

P-SV wavelengths are thus significantly shorter than P-P wavelengths within the Marcellus Shale interval.

Marcellus structural interpretation

Structural complexity increased within the Marcellus interval. Both P-P and P-SV data showed the Marcellus has a strong structural-fold fabric trending east-to-west. These linear folds were mapped and correlated in both P-P and P-SV data volumes to better understand local effects of tectonic stress on the Marcellus. Although the natural fracture pattern within the Marcellus Shale is below the resolution of these post-stack seismic data, these structure maps provide a partial understanding of probable Marcellus fracture patterns. Understanding stress fields is useful for determining where natural fractures

should be localized and for predicting how embedded fractures may behave when reactivated during hydraulic fracture treatments, or when pore pressure is altered because of fluid injections.

Similar fold patterns occur in both the Upper and Lower Marcellus units, but folds within the Lower Marcellus have slightly larger vertical relief than do their equivalents in the Upper Marcellus. These differences in fold height imply stresses acting on the Lower Marcellus may have been greater than stresses that generated folds in the Upper Marcellus. Folds are evident on P-P data (Fig. 12) but are more pronounced in P-SV_1 data (Fig. 13) and P-SV_2 data (Fig. 14). Because of the limited size of our 3D/3C seismic survey (9 mi² [23 km²] of image space), we cannot demonstrate that the structural complexities associated with the Marcellus Shale are associated with any specific regional orogenic event (for example, Taconian or Acadian), or if they are caused by more recent neotectonic joint systems formed during regional uplifting.

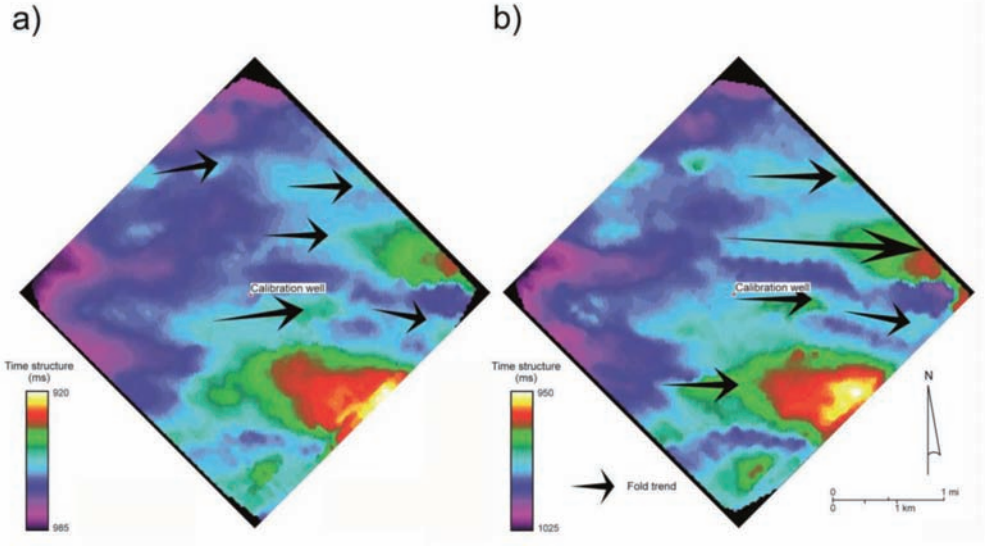

Fig. 12. (a) Upper Marcellus Shale P-P time structure. (b) Lower Marcellus Shale P-P time structure. The arrows depict orientations of fold hinges.

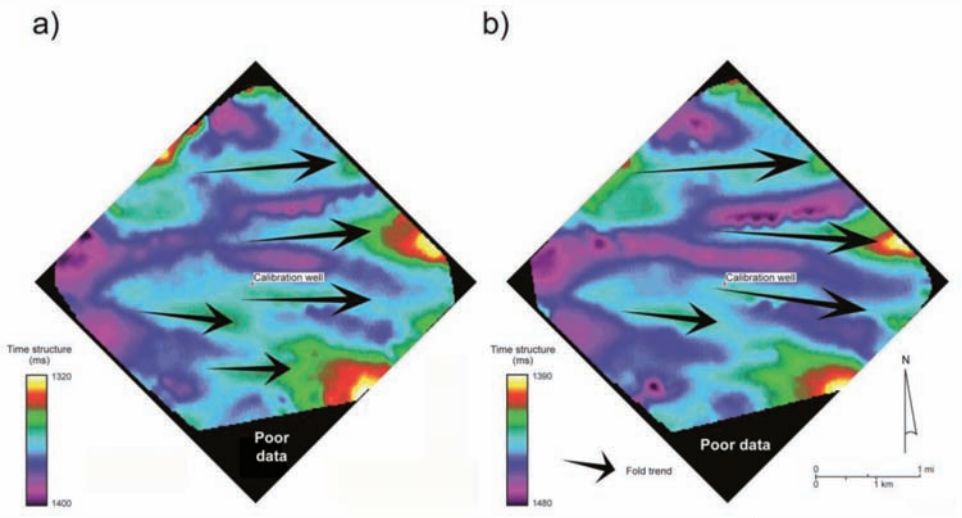

Fig. 13. (a) Upper Marcellus Shale P-SV_1 time structure. (b) Lower Marcellus Shale P-SV_1 time structure. The arrows depict orientations of fold hinges.

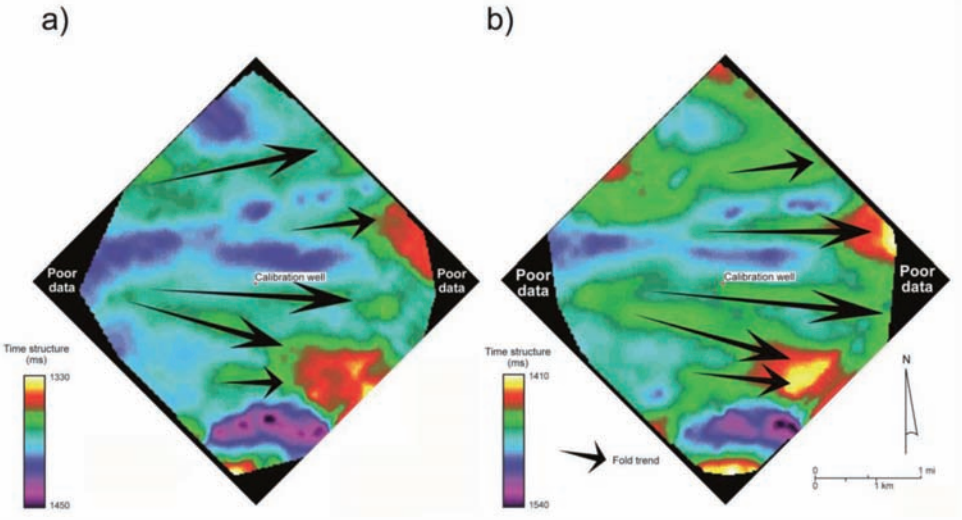

Fig. 14. (a) Upper Marcellus Shale P-SV_2 time structure. (b) Lower Marcellus Shale P-SV_2 time structure. The arrows depict orientations of fold hinges.

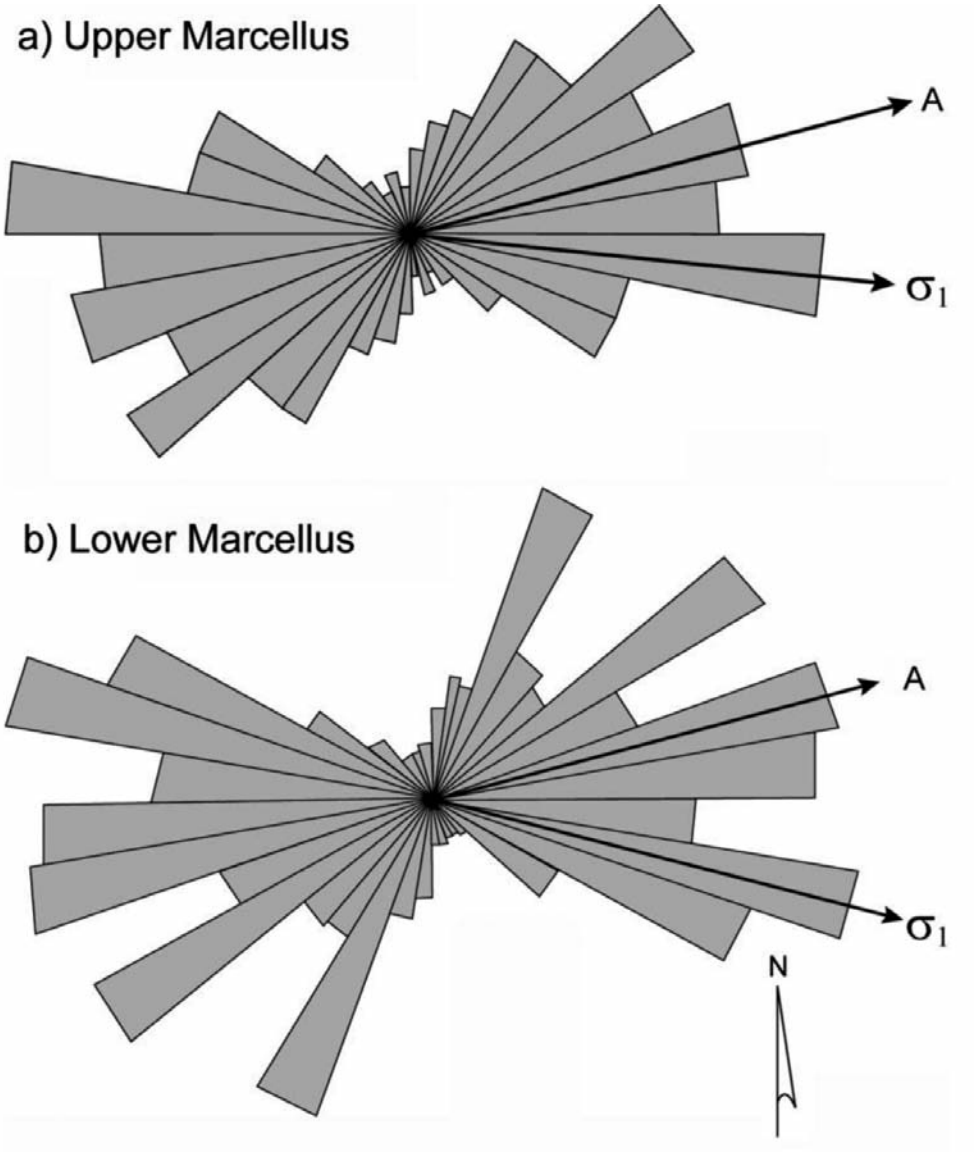

Fig. 15. Rose diagrams calculated from borehole image logs acquired in the central-image calibration well for (a) Upper Marcellus and (b) Lower Marcellus. The symbol σ_1 defines the orientations of extensional fractures interpreted from these rose diagrams. Shear fractures are oriented in a direction that is usually in a direction approximately 30-degrees away from σ_1, such as the fractures sets labeled A.

The relationship between natural fracture orientations and present-day stress are important factors in well planning for hydraulic fracturing. The orientation of natural fractures was evaluated in the central calibration well where a shear wave anisotropy log was acquired. Rose diagrams of interpreted fracture orientations generated by the logging contractor show fracture orientations in the Upper Marcellus and Lower Marcellus (Fig. 15) range from slightly south of east-west to approximately 45-degrees north of east-west. The orientations of extensional fractures (σ_1) and shear fractures (A) drawn on the rose diagrams are our interpretations of the fracture patterns, not the contractor's interpretation. If this fracture interpretation is implemented, the direction of maximum horizontal stress would be emanating approximately from the north. A significant fact implied by these rose diagrams and by the preceding structure maps is that most fractures within the Marcellus interval are oriented parallel to fold axes. Fracture set A labeled on each display is our interpretation of possible shear fractures, which typically are oriented approximately 30-degrees away from the extensional fractures created by maximum horizontal stress.

Numerous horizon-constrained seismic attributes were generated during our interpretation of the Upper Marcellus and Lower Marcellus intervals. The objective of this amplitude-attribute analysis was to determine if any amplitude calculations derived from post-stack data volumes would provide additional evidence of faulting, fracturing, or jointing within the Marcellus Shale interval. We found no amplitude attribute that provided structural, faulting, or fracturing information about the Marcellus that differed from information shown by structural maps (Figs. 12 to 14).

Marcellus P-SV wave anisotropy

Vertical fractures, when consistently oriented across an interval, cause that interval to be an azimuthally anisotropic seismic propagation medium. Because the mechanical strength of such a medium is stronger parallel to fractures than it is perpendicular to fractures, a seismic mode exhibits a faster propagation velocity parallel to fractures than it does perpendicular to fractures. This difference in propagation velocities is more pronounced for P-SV waves than it is for P-waves. For this reason, azimuthal anisotropy is often referred to as P-SV wave anisotropy. The quantity S_{ANI} will be used to indicate seismic-based P-SV wave anisotropy is defined as,

$$S_{ANI} = (V_1 - V_2)/V_2 \ , \tag{3}$$

where V_1 is fast-S velocity and V_2 is slow-S velocity. If fast-S and slow-S images of a targeted anisotropic interval are available, seismic-based interval values of V_1 and V_2 can be approximated as,

$$V_1 = D/\Delta T_1 \text{ and } V_2 = D/\Delta T_2 \ , \quad (4)$$

where D is the thickness of the interval, ΔT_1 is the time thickness of the interval on a fast-S image, and ΔT_2 is the time thickness of the interval on a slow-S image. Substituting eq. (4) into eq. (3) leads to a simple calculation that transforms fast-S and slow-S post-stack seismic data into estimates of seismic-based P-SV wave anisotropy:

$$S_{ANI} = (\Delta T_2/\Delta T_1) - 1 \ . \quad (5)$$

We calculated this quantity, S_{ANI}, across the Upper Marcellus and Lower Marcellus intervals. Maps of these seismic-based estimates of P-SV wave anisotropy are displayed on Fig. 16.

Anisotropy measurements taken at the calibration well are: Upper Marcellus 1.7% and the Lower Marcellus 1.6%, respectively. At the location of the calibration well, the Upper Marcellus has an east-to-west trending anisotropy zone of approximately 2.5-percent immediately north of the well location. The Lower Marcellus shows a northwest-to-southeast trending anisotropy zone of approximately 2-percent that passes immediately south of the calibration well. The areas highlighted with green-red-to-yellow colours have slightly higher P-SV wave anisotropy and may define localized increases in fracture intensity.

The P-SV wave anisotropy values shown on Fig. 16 are sensitive to subtle variations in the position of the Cherry Valley interface that separates Upper and Lower Marcellus. Because the Cherry Valley Limestone could not be interpreted with automatic horizon-picking algorithms, manual intervention by an interpreter was required to define the position of this thin intra-Marcellus limestone. This interpreter action may introduce some ambiguity in the position of the boundary separating Upper and Lower Marcellus.

CONCLUSIONS

The 3C/3D seismic data used in this study provided the most dramatic contrast between P-wave and P-SV wave imaging of geologic targets that our research teams has observed in the 12 years our laboratory has been engaged in multicomponent seismic interpretation. The impressive aspect of these data was that both the $P\text{-}SV_1$ (fast-S) mode and $P\text{-}SV_2$ (slow-S) mode provided better spatial resolution of key geologic targets than did P-P (compressional) data. The latter data (P-P) are the principal seismic data used to evaluate shale-gas prospects. The increase in $P\text{-}SV_1$ resolution over P-P resolution was particularly significant, with $P\text{-}SV_1$ wavelengths being approximately 40-percent shorter than

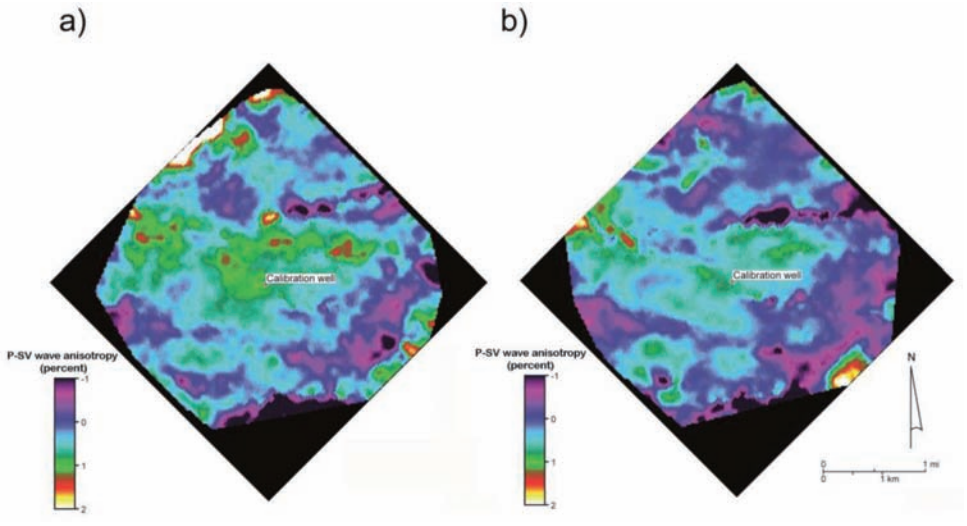

Fig. 16. P-SV wave anisotropy calculated for (a) Upper Marcellus and (b) Lower Marcellus.

P-P wavelengths. Research findings discussed in this chapter should be considered by all shale-gas operators in the Appalachian Basin so they can take advantage of the increased resolution of P-SV-shear modes relative to P-wave data. Results equivalent to ours should occur wherever the overburden above the Marcellus is similar to overburden properties where our data were acquired.

In addition to P-SV wave data providing better resolution of geologic targets, we found P-SV wave images described reservoir heterogeneities that P-P data could not see. Specifically, a channel-like feature was imaged in the Tully-to-Tichenor interval by P-SV_1 data, and no indication of the feature existed in P-P data. This finding is important because this interval contains attractive sandstones that can be utilized as reservoirs for injecting flow-back waters produced during hydrofrac operations. If units are considered for water-storage purposes, it is essential to know all heterogeneities internal to the unit to understand reservoir compartmentalization. We conclude it is essential that multicomponent seismic data be used whenever an Appalachian Basin operator is searching for potential water-injection reservoirs.

All three data volumes (P-P, P-SV_1, and P-SV_2) showed linear folds existed in the Marcellus Shale. These fold trends were not observed in the stiff

rocks above and below the Marcellus. The approximate east-west orientation of these folds agreed with the orientation of Marcellus fractures interpreted in borehole image logs acquired in the central-image calibration well. The consistent fold orientations across seismic image space imply Marcellus fracture properties should be reasonably consistent across the image area.

Isopach thicknesses of P-SV_2 and P-SV_1 images across the Marcellus were combined to estimate P-SV wave anisotropy within the Marcellus. This anisotropy attribute is important because it is a qualitative indicator of fracture intensity. Seismic-based anisotropy values were small, of the order of 1 to 2 percent, which were the same values calculated from fast-S and slow-S modes measured with a dipole sonic log acquired in the central-image well. This seismic result is both encouraging and discouraging. It is encouraging because seismic-based estimates of anisotropy agree with values defined by calibration logs. The result is discouraging because it incorrectly implies few fractures are present in the Marcellus.

As we began to understand the Marcellus had orthogonal joint sets, we began to question how P-SV wave data would differ when orthogonal joints were widely spaced versus when the joints were closely spaced. In this type of medium, the best indicator of orthogonal-joint intensity appears to be the magnitude of VS velocity across the Marcellus. Where joint intensity increases, VS interval velocity should decrease. Where joint intensity decreases, VS interval velocity should increase. We thus abandon the use of P-SV wave anisotropy for predicting joint intensity in the Marcellus and propose a new attribute - VS_2 interval velocity - for mapping increases and decreases in joint intensity.

ACKNOWLEDGEMENTS

This article was prepared with the support of the Research Partnership to Secure Energy for America (RPSEA) under Project No. 08122-55. However, any opinions, findings, conclusions, or recommendations expressed herein are those of the authors and do not necessarily reflect the views of RPSEA. Support for this work was provided in part by the John A. and Katherine G. Jackson School of Geosciences and the Geology Foundation at The University of Texas at Austin. As an industry partner, Geokinetics and Geophysical Pursuit provided the 3C/3D seismic data; Chesapeake Energy provided the digital well logs and VSP data. Landmark Graphics Corporation provided software for the basic 3C/3D seismic interpretation via the Landmark University Grant Program. The illustrations were prepared with the assistance of Cathy Brown, Manager of Media Services and the BEG Graphics Section. Publication was authorized by the Director, Bureau of Economic Geology, The University of Texas at Austin.

REFERENCES

Bruner, K.R. and Smosna, R., 1994. Porosity development in Devonian lithic sandstones of the Appalachian foreland basin. Northeast. Geol., 16: 202-214.

DeAngelo, M.V., Backus, M., Hardage, B., Murray, P. and Knapp, S., 2003. Depth registration of P-wave and C-wave seismic data for shallow marine sediment characterization, Gulf of Mexico. The Leading Edge, 22: 96-105.

Diecchio, R.J., 1985. Post-Martinsburg Ordovician stratigraphy of Virginia and West Virginia. Virginia Div. Mineral Res., Publicat. 57: 77 pp.

Engelder, T., Lash, G.G. and Uzcátegui, R.S., 2009. Joint sets that enhance production from Middle and Upper Devonian gas shales of the Appalachian Basin. AAPG Bull., 93: 857-889, doi:10.1306/03230908032.

Hill, C.G., 2002. Fractured Shale Gas Potential in New York. Rep. New York State Energy Res. Develop. Author.: 1-49.

Milici, R.C. and Swezey, S., 2006. Assessment of Appalachian Basin oil and gas resources: Devonian shale - Middle and Upper Paleozoic total petroleum system. USGS Open-File Rep. 2006-1237: 70 pp.

Roen, J.B., 1984. Geology of the Devonian Black Shales of the Appalachian basin. Organ. Geochem., 5: 241-254.

Soeder, D.J., 1988. Porosity and permeability of eastern Devonian gas shale. Soc. Petrol. Engin. Format. Evaluat., SPE, 3: 116-124, doi: 10.2118/15213-PA.

Tatham, R.H. and McCormick, M.D., 1991. Multicomponent Seismology in Petroleum Exploration. SEG, Tulsa: 248 pp.

Zeng, H., Henry, S.C. and Riola, J.P., 1998. Stratal slicing, Part II: Real seismic data. Geophysics, 63: 514-522.

Zeng, H., Hentz, T.F. and Wood, L.J., 2001. Stratal slicing of Miocene-Pliocene sediments in Vermilion block 50 - Tiger Shoal area, offshore Louisiana. The Leading Edge, 20: 408-418.